Physics in Medicine & Biology

IPEM Institute of Physics and Engineering in Medicine

ACCEPTED MANUSCRIPT • OPEN ACCESS

Towards liquid EPR dosimetry using nitroxides in aqueous solution

To cite this article before publication: Sebastian Höfel *et al* 2024 *Phys. Med. Biol.* in press https://doi.org/10.1088/1361-6560/ad25c4

Towards liquid EPR dosimetry using nitroxides in aqueous solution

Sebastian Höfel[1,2], Felix Zwicker[2,3,4], Michael K. Fix[5], Malte Drescher[1]

[1] Department of Chemistry and Konstanz Research School Chemical Biology, University of Konstanz, Konstanz, Germany

[2] Klinik und Praxis für Strahlentherapie am Klinikum Konstanz, Konstanz, Germany

[3] Department of Radiation Oncology, Heidelberg University Hospital, Heidelberg, Germany

[4] Clinical Cooperation Unit Molecular Radiation Oncology, German Cancer Research Center (DKFZ), Heidelberg, Germany

[5] Division of Medical Radiation Physics and Department of Radiation Oncology, Inselspital, Bern University Hospital and University of Bern, Switzerland

Address all correspondence to:

Prof. Dr. Malte Drescher
Department of Chemistry
University of Konstanz
Box 706, Universitätsstraße 10
78457 Konstanz, Germany
Phone: +49 7531 88-5262
Email: malte.drescher@uni-konstanz.de

Abstract

Objective: Water-equivalent dosimeters are desirable for dosimetry in radiotherapy. The present work investigates basic characteristics of novel aqueous detector materials and presents a signal loss approach for electron paramagnetic resonance (EPR) dosimetry.

Approach: The proposed principle is based on the radiation dose dependent annihilation of EPR active nitroxides (NO·) in aqueous solutions. Stable nitroxide radicals (3-Maleimido-2,2,5,5-tetramethyl-1-pyrrolidinyloxy (MmP), 3-Carbamoyl-2,2,5,5-tetramethyl-1-pyrrolidinyloxy (CmP)) in aqueous solutions containing dimethyl sulfoxide (DMSO) as an additive were filled in glass capillaries for irradiation and EPR readout. Radiation doses ranging from 1 – 64 Gy were applied with a clinical 6 MV FFF photon beam. EPR readout was then performed with a X-band benchtop spectrometer. The dose response, temporal stability and reproducibility of the samples' EPR signal amplitudes as well as the influence of the nitroxide concentration between 10 – 160 µM on the absolute signal loss were investigated using MmP. CmP was used to examine the dependence of the dose response on DMSO concentration between 0 – 10vol%. An indirect effect model was fitted to the experimental data assuming irradiation induced radical reactions as the underlying mechanism.

Main results: For an initial MmP concentration of 20 µM, absolute EPR signal loss is linear up to a dose of 16 Gy with a yield G(-NO·) of approximately 0.4 µmol/J. Within five weeks upon sample irradiation to doses between 0 Gy and 32 Gy relative EPR signal fluctuations were on average (126 readouts) below 1% (1σ). For c(MmP) ≥ 20 µM, absolute signal loss is only weakly dependent on c(MmP), whereas it increases strongly with increasing c(DMSO) in the range 0 - 5vol%. An indirect effect model is applicable to describe the reaction mechanism resulting in the observed dose response curve.

Significance: Liquids consisting of nitroxides in aqueous solution and small amounts of DMSO (2vol%) show promising basic characteristics for application as water-equivalent EPR dosimeter materials in radiotherapy. The EPR signal loss is based on an indirect effect mediated by diffusing radicals originating from the radiolysis of the water/DMSO mixture.

Keywords: EPR dosimetry, radiotherapy, water equivalence, nitroxide, dimethyl sulfoxide

1. Introduction

Clinical experience and dose prescriptions in radiotherapy are historically based on the dose quantity D_w, i.e. the absorbed dose-to-water. Hence, many commercial treatment planning systems report D_w values inside the patient's body, e.g. after applying density scaling to account for tissue heterogeneities if model-based dose calculation algorithms are used (Papanikolaou *et al.* 2004, Ma and Li 2011).

Consistently, clinical dosimetry typically aims to determine D_w values in water or water-equivalent materials by means of probe detectors (Almond *et al.* 1999, IAEA 2001). For water-equivalent materials, both, physical density and atomic composition, need to be close to water in order to provide water-like radiation interaction properties (ICRU 1989, Gargett *et al.* 2020). Consequently and to minimize fluence perturbations of the radiation field, the ideal D_w probe detector should be water-equivalent as well (Nahum 1996). However, commonly used detectors (e.g air-vented ionization chambers (IC), diodes, thermoluminescence detectors (TLD) and others) cannot be considered water-equivalent and therefore require setup-specific conversion of the detector reading to the true D_w value at the point of measurement in the absence of the detector. International dosimetry protocols guide users to perform absolute D_w measurements in so-called reference conditions (IAEA 2001). Non-reference conditions usually involve the determination and application of additional detector specific correction factors to the detector reading in order to determine D_w (Chofor *et al.* 2012). This circumstance is partially caused by the lack of water equivalence of the used detector. For some non-reference conditions, correction factor determination is crucial yet challenging and subject to ongoing research e.g. dosimetry in the dose build-up region where most detectors show an over-response (Apipunyasopon *et al.* 2013, O'Shea and McCavana 2003) or dosimetry in small radiation fields (Poppinga *et al.* 2018, Fenwick *et al.* 2013). In such situations, water-equivalent dosimeters are highly desirable but dosimetry methods utilizing water-equivalent detectors are lacking.

Electron paramagnetic resonance (EPR) dosimetry has been shown to be applicable in the radiotherapy dose range (Sharpe *et al.* 1996, Anton 2005), even when following a practical protocol tailored for routine clinical use (Hoefel *et al.* 2021). So far, the EPR dosimetry principle has been based on the quantitative detection of radiation induced permanent radicals in solid detector materials such as polycrystalline L-alanine (ALA) (Regulla and Deffner 1982) or lithium formate monohydrate (LFM) (Vestad *et al.* 2004). These two materials are often considered to be water-equivalent in terms of the detector-to-water ratios of the photon mass energy absorption coefficients $\left(\frac{\mu_{en}}{\rho}\right)_{det} / \left(\frac{\mu_{en}}{\rho}\right)_{H_2O}$ as well as of the electron mass collision stopping powers $\left(\frac{S_{col}}{\rho}\right)_{det} / \left(\frac{S_{col}}{\rho}\right)_{H_2O}$. For ALA and LFM, these ratios are close to unity and vary only little over the energy range used in radiotherapy (Olsen *et al.* 1990, Vestad *et al.* 2004). In addition, EPR dosimeter response is typically independent on dose rate and angle of beam incidence (Regulla and Deffner 1982, Desrosiers *et al*. 2008, Waldeland *et al.* 2011). Consequently, a calibration factor obtained

for ALA or LFM, e.g. under reference conditions, can be applied under many non-reference conditions without further corrections (Schaeken *et al.* 2011, Distefano *et al.* 2017). ALA and LFM are commonly used in the form of pellets essentially made of polycrystalline powder. Crystals of ALA and LFM exhibit physical densities of approximately 1.4 g/ccm. Depending on the manufacturing process, typical pellet densities are between 1.2-1.3 g/ccm (Anton 2008, Antonovic *et al.* 2009) causing a non-negligible density effect, i.e. altering the dosimeter reading per absorbed-dose-to-water in situations where charged particle equilibrium is not established, e.g. in small radiation fields or in the dose build-up region (Cronholm *et al.* 2012, Fenwick *et al.* 2013).

In search of an EPR dosimeter exhibiting a water-like density, the current work introduces a novel approach for EPR dosimetry using aqueous liquids as detector materials. In contrast to conventional EPR dosimetry, the principle presented here is based on a dose dependent EPR signal loss: Stable paramagnetic species dissolved in aqueous solution are transformed into diamagnetic products upon irradiation.

The presented approach uses commercially available nitroxides (also known as aminoxyl or nitroxyl free radicals). Nitroxides have been extensively studied for decades and are well known for their applications in protein research, material science and medicine (Torricella *et al.* 2020, Kokorin 2012, Soule *et al.* 2007). To the best of our knowledge, nitroxides have not yet been utilized for EPR dosimetry in radiotherapy.

As shown in the current work, there is a notable EPR signal loss effect of micromolar aqueous nitroxide solutions irradiated to clinical doses if dimethyl sulfoxide (DMSO) is present as an additive. Based on this discovery, the current work investigates fundamental dosimetric characteristics of aqueous solutions containing nitroxides in low concentrations (10 – 160 µM) and small amounts of DMSO (0 - 10 vol%). Such mixtures are intended to be used as encapsulated probe detectors in radiotherapy. A heuristic kinetic model was established and discussed assuming reactions between nitroxides and transient radicals originating from the radiolysis of the water/DMSO mixture as the root cause for the EPR signal loss.

2. Material and Methods

Three measurement series (S1-S3) were conducted. The reproducibility of the EPR readout procedure, the temporal fading of the EPR signal intensities as well as the dependence of the EPR signal intensities on the absorbed dose were investigated in S1. In S2 and S3, the dependence of the absolute EPR signal loss on nitroxide and DMSO concentration were examined, respectively. S2 and S3 aimed to explore the nature of the mechanism behind the observed signal loss effect.

2.1 Dosimeter preparation

Ultrapure water with an electrolytic conductivity of 0.055 µS/cm was taken from a Barnstead™ Smart2Pure™ water purification system (ThermoFisher Scientific Inc., Waltham, MA, USA). Purified DMSO ROTIPURAN®≥99.8% was purchased from Carl Roth GmbH & Co. KG (Karlsruhe, Germany). Two common nitroxides 3-Maleimido-2,2,5,5-tetramethyl-1-pyrrolidinyloxy (MmP) and 3-Carbamoyl-2,2,5,5-tetramethyl-1-pyrrolidinoxy (CmP) were purchased from Sigma Aldrich (St. Louis, MO, USA). The molecular structures are depicted in Figure 1 (a). As a common feature, nitroxides possess an unpaired electron spin that is delocalized across the N-O moiety. In the fast motional regime, i.e. for nitroxides freely tumbling in a liquid solution, the hyperfine coupling with the nitrogen's nuclear spin gives rise to a characteristic three-line EPR spectrum in X-band (cf. Figure 1 (b)) (Bordignon 2017).

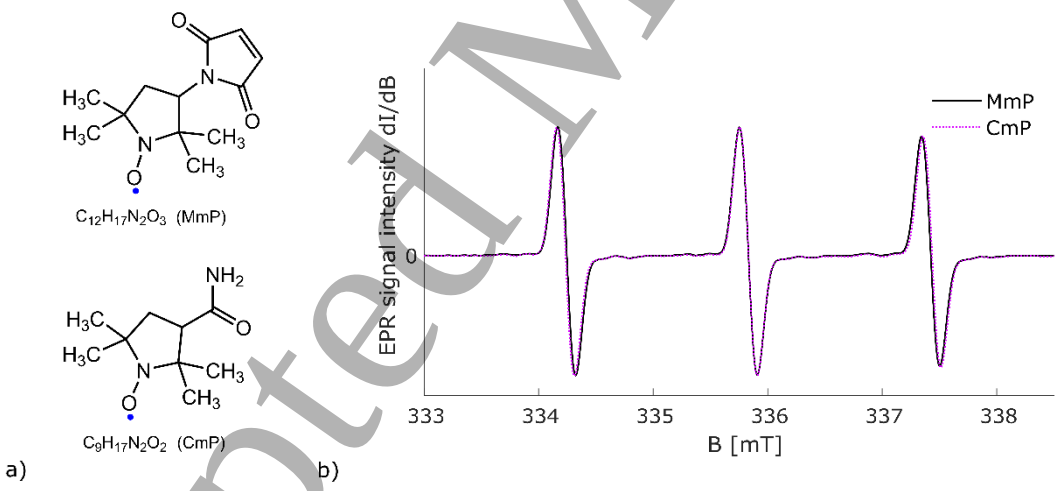

Figure 1. Chemical structures and formulas of nitroxides MmP and CmP. The location of the unpaired electron is illustrated by the blue dot (a). Room temperature (22°C) continuous wave X-band EPR spectra of MmP and CmP in aqueous solution (b).

For S1 and S2, aqueous solutions of MmP containing 2vol% DMSO were used. MmP was first dissolved in DMSO to obtain a 10 mM stock solution in 100vol% DMSO. For S2, different portions of the stock solution were mixed with ultrapure water and DMSO to obtain aqueous solutions with fixed 2vol% DMSO content

but variable MmP concentration (10, 20, 40, 80 and 160 µM). A nitroxide solution containing 20 µM MmP, 2vol% DMSO and 98vol% ultrapure water was used for S1.

Aqueous solutions of CmP were used for S3. In contrast to MmP, Cmp is directly soluble in water. CmP was thus directly dissolved in 100vol% ultrapure water to obtain a 10 mM stock solution. By dilution and adding different amounts of DMSO, nitroxide solutions containing 20 µM CmP but variable amounts of DMSO (0, 0.01, 0.02, 0.05, 0.1, 0.2, 0.5, 1, 2, 5 and 10 vol% DMSO) were prepared. Nitroxides in aqueous solutions are hereinafter referred as "nitroxide solution".

For irradiation and for EPR readout the nitroxide solutions were filled in glass capillaries (50 µL ringcaps® from Hirschmann Laborgeräte GmbH & Co. KG, Eberstadt, Germany) and sealed with Critoseal® capillary tube sealant from Leica Microsystems GmbH (Wetzlar, Germany). Direct contact between the nitroxide solution and the sealant was avoided by an air column (cf. Figure 2 (a)). The capillaries are made of borosilicate glass (DURAN®) with an inner and outer diameter of 1.0 mm and 1.6 mm, respectively. A "sample" was defined as a capillary filled with a minimum volume of 25 µL nitroxide solution corresponding to a filling height of approximately 3 cm. The solutions and samples were stored at room temperature. During sample preparation for the current work, oxygen was not removed from the nitroxide solution. Thus, a molecular oxygen concentration of approximately 0.28 mM can be assumed corresponding to the saturation level of 9 mg/L at room temperature and normal pressure.

2.2 Irradiation

All samples were irradiated by a clinical 6 MV flattening filter free (FFF) photon beam of a Halcyon™ (Varian Medical Systems, Palo Alto, CA, USA) treatment system at room temperature 22 ± 1 (1σ) °C. The samples were placed at 1.5 cm depth inside a solid water slab phantom with a size of 55 x 15 x 12 cm³. The beam was directed perpendicular to the phantom surface positioned at 100 cm source-surface distance. A square radiation field size of 10 cm x 10 cm was used for all irradiations. The monitor unit (MU) rate was 800 MU per minute resulting in a dose rate of about 8.0 Gy/min at the sample location for the used output calibration. The radiation beam of the Halcyon's clinical linear accelerator (LINAC) is delivered in pulsed mode with a repetition frequency of 167 Hz and a pulse (burst) duration of approximately 4.2 µs (FWHM). These values were taken from the service mode display. Based on this information, a dose per burst D_b of about 0.8 mGy and an instantaneous dose rate of 0.19 kGy/s could be derived.

2.3 EPR readout

EPR measurements were performed in continuous wave (CW) mode using a benchtop spectrometer (MiniScope MS 5000, Magnettech by Freiberg Instruments GmbH, Freiberg, Germany) operating in

X-band. The MiniScope uses a rectangular TE102 resonator that provides a high magnetic field intensity but low electric field intensity at the resonator center where the EPR sample is typically placed, thereby increasing EPR absorption (i.e. signal intensity) and reducing microwave power dissipation due to dielectric loss (Webb 2014). In the present work, glass capillaries are used as sample vessels to minimize dissipative effects during EPR readout – as typically done in EPR spectroscopy when dealing with aqueous samples. Due to the inhomogeneity of the electromagnetic field distribution inside the TE102 cavity, exact positioning of the sample inside the resonator is crucial for quantitative and reproducible EPR measurements. A double tapered guidance tube, a stopper and a minimum sample filling height helped to reduce positioning uncertainties as described in the following.

The samples were inserted vertically into the resonator as illustrated in Figure 2 (b). A double tapered guidance tube was installed in a fixed position thereby minimizing lateral positional uncertainties of the samples. The guidance tube was open at both ends enabling a temperature controlled nitrogen gas flow around the sample (see below). A porous stopper was used at the bottom end of the guidance tube to fix the vertical position of the inserted sample. The volume within the sample capillary where the magnetic field intensity of the standing microwave is non-zero, i.e. the sensitive volume, has a height of approximately 3 cm. The samples used were filled such that the liquid column completely covered the sensitive volume (cf. section 2.1). The influence of the exact start and endpoint of the liquid column on the signal intensity was thereby eliminated.

A microwave power of 2 mW and a 100 kHz B_0-field modulation with an amplitude of 0.16 mT were applied. The chosen modulation amplitude maximized the signal-to-noise ratio. The microwave power setting assured operation in the linear regime, where the EPR intensity increases linearly with the square root of the microwave power. The scan range and sweep time were 12 mT and 60 s, respectively, and a total of 5 consecutive scans were acquired and averaged per measurement. Auto-tuning of the resonator coupling before each scan was enabled. Using these readout parameters and for the dose range and capillaries investigated in the present work, there was no disturbing radiation induced EPR signal in the glassware observable.

A temperature controller (TC) TCH04 from Magnettech by Freiberg Instruments GmbH (Freiberg, Germany) was used to perform the EPR measurements under controlled temperature conditions since the linewidth of the nitroxides' EPR spectrum is sensitive to temperature changes (Bordignon 2017, Bales *et al.* 2009). The TC consists of a vessel containing liquid nitrogen and two software controlled components: An evaporator and a heater. A temperature sensor is used at the outlet providing feedback to control a specified temperature value. All EPR readouts were performed at T = 22°C. The temperature controlled nitrogen gas flow enters the resonator cavity from below via a glass dewar and flows around the sample capillary (Figure 2 (b)). The gas flow exits the sample guidance tube at the top end and is

redirected into the resonator cavity by using a hose. Flushing the cavity with nitrogen gas aimed at removing possible moisture inside the cavity that affects the sensitivity of the spectrometer.

A manganese ($ZnS:Mn^{2+}$ powder (cubic zincblende structure)) intensity reference substance (Magnettech by Freiberg Instruments GmbH, Freiberg, Germany) was present in the resonator cavity (Figure 2 (b)) during all measurements. By applying the chosen magnetic field sweep range, the middle two lines of the manganese six-line EPR spectrum were recorded together with the nitroxide spectrum.

All irradiated samples were measured on the day of irradiation. The S1 samples were additionally readout weekly within five weeks following irradiation, i.e. 2, 9, 16, 23 and 30 days after irradiation.

The total measuring time per sample readout was about 7 minutes including a so called setup time of 2 minutes before the first scan to enable temperature equalization.

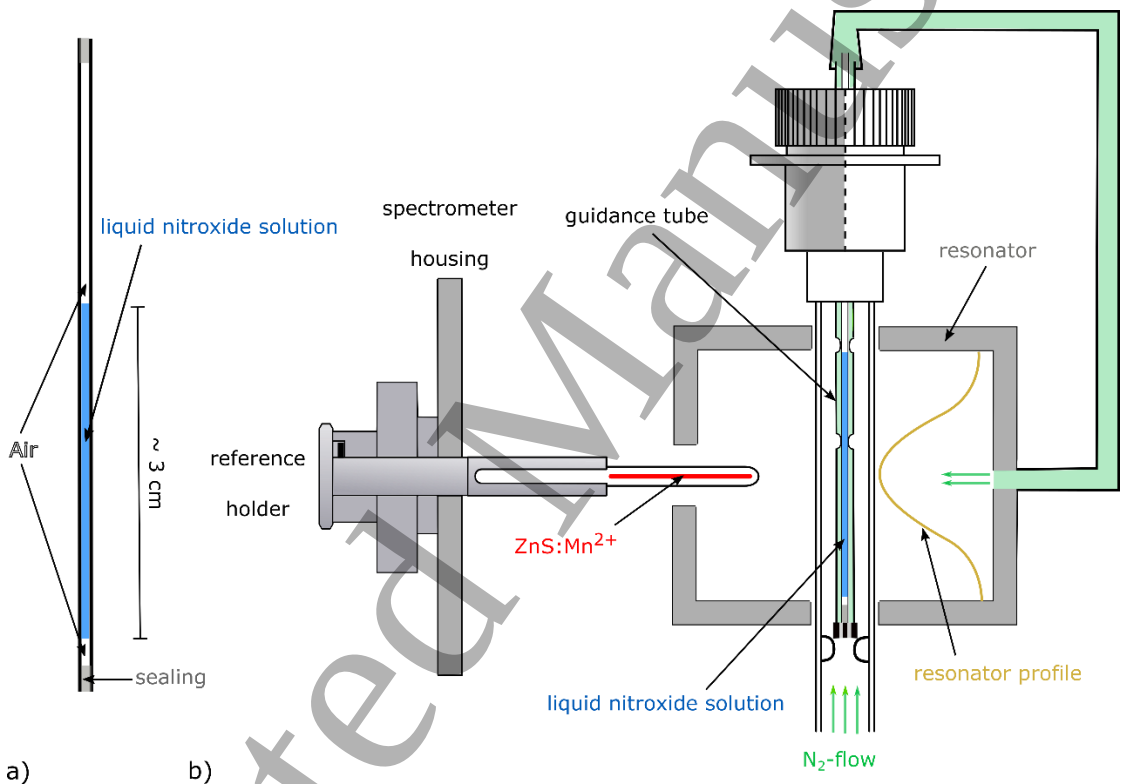

Figure 2. Filled capillary tube (sample) showing the liquid nitroxide solution (blue), sealing (grey) and air columns (white) (a). Sketch of the EPR measurement setup (b). Sample vertically inserted into the resonator and temperature controlled by a nitrogen gas flow (green). Porous stopper shown in black. Vertical distribution of magnetic field intensity inside the resonator, i.e. the resonator profile (yellow). A manganese reference substance (red) is inserted from the side of the spectrometer and is measured simultaneously.

2.4 Spectral evaluation

The evaluation was based on the determination of signal amplitudes following an established spectral fitting procedure outlined in a previous work (Hoefel *et al.* 2021). For the purpose of the current work, the procedure was adapted to liquid nitroxide solutions as follows.

The measured EPR spectrum S is to be interpreted as a superposition (equation (1)) of a pure nitroxide spectrum R and a manganese spectrum Mn (section 2.3). Besides, an inevitable baseline drift is present as underlying background signal BG.

$$S = R + Mn + BG = a\,R^B + b\,Mn^B + BG \tag{1}$$

The amplitudes of the Mn signal and the R signal were evaluated by fitting base spectra (R^B, Mn^B) to the composite spectrum S using a least-squares optimization in MATLAB® (MathWorks, Nattick, MA, USA). Figure 3 exemplarily shows the spectral relations between S and the two base spectra. The resulting fit coefficients (a and b) reflect the amplitude scaling factors for R^B and Mn^B, respectively, in order to reproduce S via equation (1).

In the current work, pure radical base spectra R^B were determined from EPR measurements of samples containing nitroxide solutions with a concentration $c^0_{NO\cdot}$ of 20 µM. The manganese base spectrum Mn^B was acquired for 30 min with a sample containing no nitroxides but corresponding amounts of DMSO and water as the sample under investigation. In addition to the pure Mn spectrum, the Mn^B base spectrum included small EPR signal contributions from the resonator and the glass ware. The BG signal was modeled by a first order polynomial function.

Since the reproducibility of absolute EPR intensities is affected by sensitivity fluctuations of the spectrometer, precise EPR dosimetry protocols evaluate signal amplitudes in relation to an appropriate intensity reference signal (Anton 2005, Hoefel *et al.* 2021). The normalized EPR signal amplitude A_n defined in equation (2) is therefore used as a more reliable measure of the nitroxide spin concentration.

$$A_n = \frac{a}{b} \tag{2}$$

The nitroxide spin concentration of a sample is obtained by multiplying A_n with the spin concentration of the base spectrum.

$$c_{NO\cdot} = A_n\, c^0_{NO\cdot} \tag{3}$$

Statements on the EPR signal loss refer to changes in A_n instead of a. The absolute EPR signal loss ΔA_n is determined by subtracting the A_n value of the irradiated sample from the A_n value of the corresponding non-irradiated sample.

There was no correction for sample mass or volume applied, since the sensitive volume was always completely filled (cf. section 2.3) and the relative standard deviation of the sample volume among different capillaries was smaller than 0.5%.

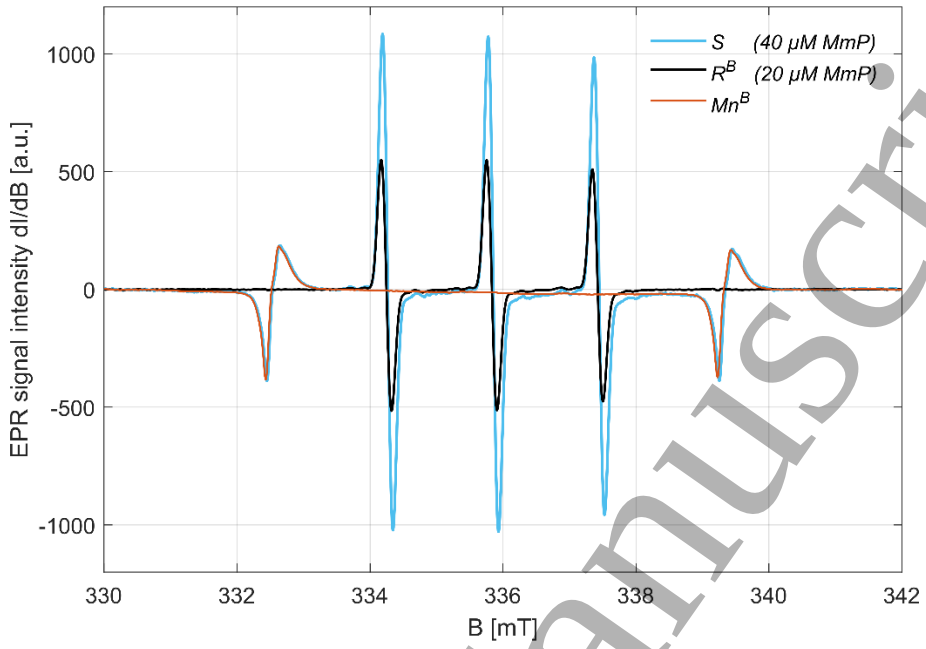

Figure 3. Example of a measured spectrum S (blue) resulting from a 40 µM MmP sample and corresponding base spectra R^B (black) and Mn^B (red) used for the spectral fitting procedure.

2.5 Modelling direct effects

To model potential direct effects of ionizing radiation on nitroxide molecules dissolved in aqueous solution, it is assumed that inactivation of a nitroxide may be caused by a single energy absorption event within the nitroxide molecule and that the probability of such an event (hit) is proportional to the absorbed dose as well as proportional to the nitroxide concentration. Let $c_{NO\cdot}$ be the concentration (mole per volume V) of nitroxides and let D be the total mean dose absorbed in volume V. The incremental change in concentration $dc_{NO\cdot}$ per dose increment dD is then proportional to the current concentration $c_{NO\cdot}$:

$$\frac{dc_{NO\cdot}}{dD} = -\,k\,c_{NO\cdot} \tag{4}$$

The proportionality factor k comprises the molar mass $M_{NO\cdot}[\mathrm{kg/mol}]$ of the nitroxide molecule and the hypothetical radiolytic yield for the direct effect $G_{DE}(-NO\cdot)$ $[\mathrm{mol/Joule}]$ that is defined as the average number of nitroxides annihilated per absorbed energy

$$k = M_{NO\cdot}\; G_{DE}(-NO\cdot)\,. \tag{5}$$

Solving equation (4) via integration with initial concentration $c^0_{NO\cdot}$ results in

$$c_{NO\cdot}(D) = c^0_{NO\cdot}\, e^{-kD}\ . \tag{6}$$

This is in accordance with the well-known exponential "survival" function alternatively resulting from a single-hit/single-target model for small hit probabilities, i.e. low target concentrations (Alpen 1998). Consequently, the concentration decrease $\Delta c_N(D)$ for a given dose is proportional to $c^0_{NO\cdot}$:

$$\Delta c_{NO\cdot}(D) = c^0_{NO\cdot} - c_{NO\cdot}(D) = c^0_{NO\cdot}\,(1 - e^{-kD}) \tag{7}$$

Note that the absolute EPR signal loss ΔA_n is proportional to nitroxide concentration changes $\Delta A_n \propto \Delta c_{NO\cdot}(D)$ (cf. equation (3)). Thus, if a direct effect is responsible for the annihilation of the nitroxide EPR signal, ΔA_n will be proportional to $c^0_{NO\cdot}$ as well.

2.6 Modelling indirect effects

The idea of the following heuristic kinetic model is to describe the irradiation induced EPR signal loss of dissolved nitroxide molecules by an indirect effect based on radiation induced radical reactions. For this situation, it is assumed that the ionizing photon beam interacts exclusively with solvent molecules, i.e. the water/DMSO mixture, thereby generating a radical species $R\cdot$ with radiolytic yield $G(R\cdot)$ [mol/Joule]. We further assume that these radicals diffuse through the mixture and chemically react via three possible channels (c.f. Figure 4): i) Second order reaction with the NO· radicals (rate constant k_1 [L/(mol·s)]) thereby forming diamagnetic products (EPR signal loss) with yield $G_{IE}(-NO\cdot)$, ii) pseudo first order reaction with the solvent or dissolved gases (e.g. O_2) (rate constant k_2 [1/s]) leading to unreactive products or iii) second order reaction between $R\cdot$ radicals with rate constant k_3 [L/(mol·s)]. The second reaction channel is assumed to be of pseudo first order, i.e. the reaction rate is not depending on the solvent concentration, since the dose dependent concentration changes of the solvent molecules are negligible for the dose values applied in this work.

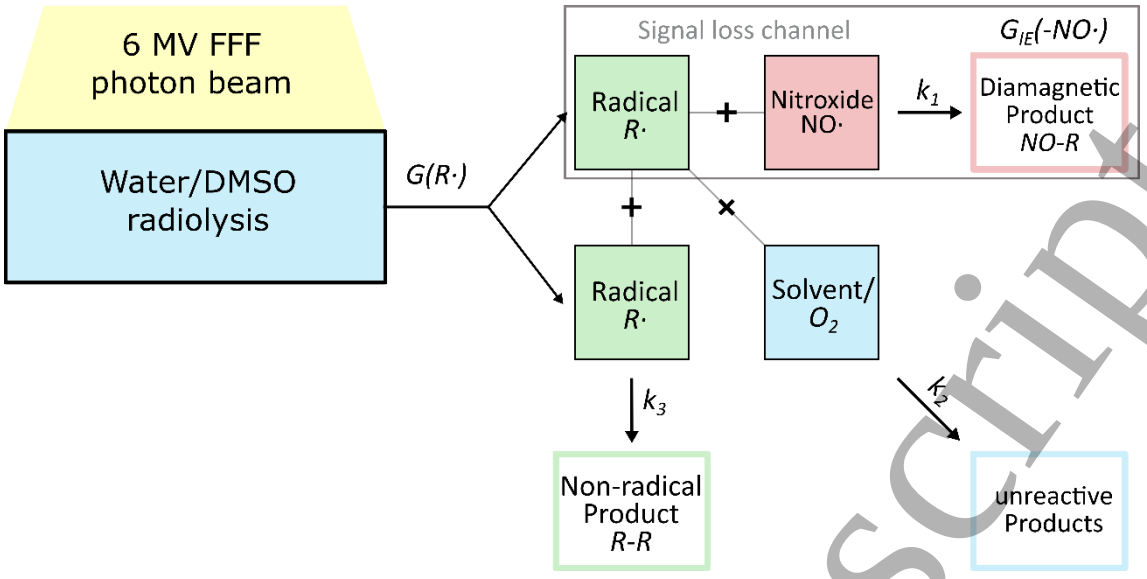

Figure 4. Diagram of the proposed indirect effect model. The photon beam is interacting with the solvent (water/DMSO mixture) generating radicals $R\cdot$ with yield $G(R\cdot)$ that diffuse and react via three different channels: i) with the dissolved nitroxides molecules (reaction constant k_1) forming diamagnetic products with yield $G_{IE}(-NO\cdot)$, ii) with the solvent or dissolved gases (e.g. O_2) (reaction constant k_2) forming unreactive products or iii) with another radical $R\cdot$ (reaction constant k_3) resulting in non-radical products.

It is further assumed that the applied photon beam generates a fix concentration of radicals $[R\cdot]_b$ instantaneously by each photon burst. $[R\cdot]_b$ is derived from the dose per burst D_b (cf. section 2.2) via

$$[R\cdot]_b = D_b\, G(R\cdot)\, \rho \tag{8}$$

with the solvent density ρ, which is set to 1.0 kg/L for the water/DMSO mixture. The modeled remaining nitroxide concentration $[NO\cdot]$ is a function of the total number of bursts, i.e. the applied total dose. To model the dose dependent decrease of $[NO\cdot](D)$ the following system of ordinary differential equations (SODE) is solved iteratively (iteration variable i) after each photon burst.

$$\frac{d[R\cdot]_i}{dt} = -k_1[R\cdot]_i[NO\cdot]_i - k_2[R\cdot]_i - k_3[R\cdot]_i^{\,2} \tag{9}$$

$$\frac{d[NO\cdot]_i}{dt} = -k_1[R\cdot]_i[NO\cdot]_i \tag{10}$$

Stepwise numerical integrations via a Runge-Kutta method was applied (MATLAB function *ode45*). After the burst repetition time of 6 ms (167 Hz burst frequency) the SODE is solved again from timepoint $t = 0$.

The start conditions $[R\cdot]_i(t=0)$ and $[NO\cdot]_i(t=0)$ are defined as follows: For the first initial iteration, the start conditions were set to $[R\cdot]_1(t=0)=[R\cdot]_b$ and $[NO\cdot]_1(t=0)=c^0_{NO\cdot}$.

For the subsequent iterations, the start conditions were

$$[R\cdot]_i(t=0)=[R\cdot]_b+[R\cdot]_{i-1}(t=6\,\mathrm{ms}) \quad (11)$$

$$[NO\cdot]_i(t=0)=[NO\cdot]_{i-1}(t=6\,\mathrm{ms}). \quad (12)$$

For simulating the dose dependence of $[NO\cdot]$ up to 64 Gy, about 80.000 iteration steps were required. The model parameters were $G(R\cdot)$, k_1, k_2 and k_3. Different values of the parameter set were tested to simulate the dose dependence $[NO\cdot](D)$ which is proportional to the measured dose dependence $A_n(D)$ (cf. equation (3)).

3. Results

3.1 Dose response and temporal stability

Figure 5 shows EPR spectra of the measurement series S1 (20 µM MmP in 2vol% DMSO and 98 vol% ultrapure water) acquired on the day of irradiation (day 0). The shown samples were irradiated to different doses ranging from 0 to 64 Gy. A monotonous dose dependence was observable, i.e. nitroxide EPR signal amplitudes decreased with increasing dose. At a dose of 64 Gy, the normalized EPR signal Amplitude A_n was reduced to 0.1. According to equation (3), the nitroxide concentration was reduced to 2 µM corresponding to 10% of the initial concentration of 20 µM.

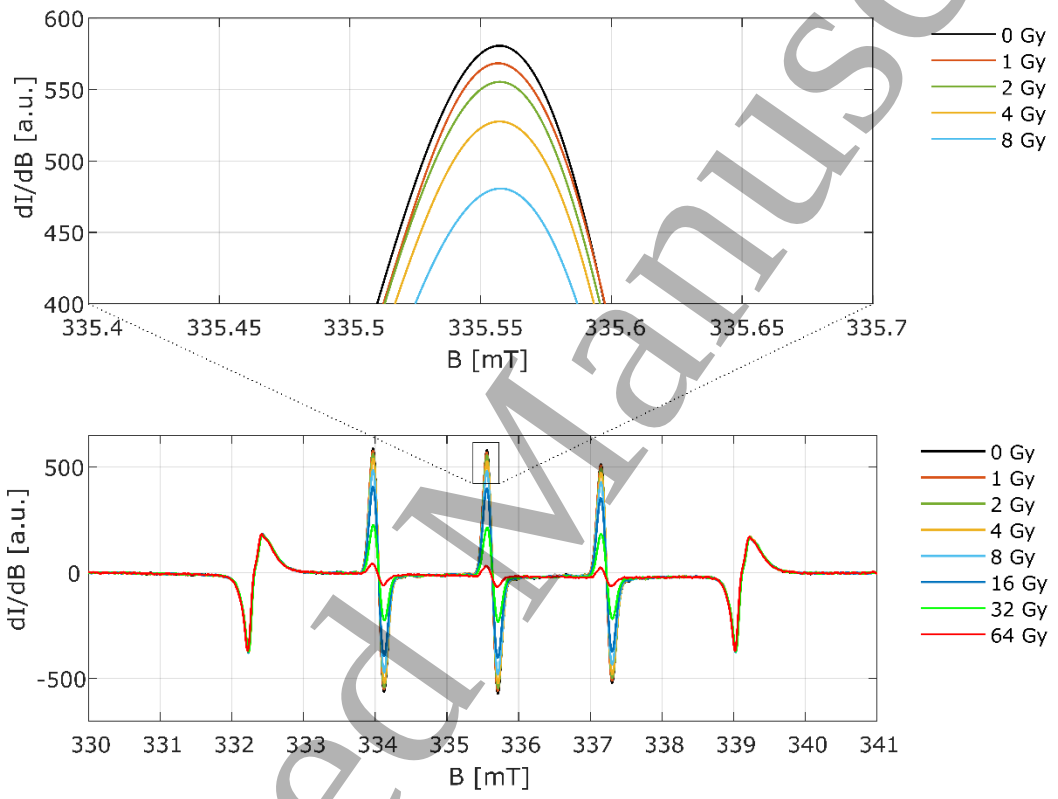

Figure 5. Dose dependent decrease of the nitroxide EPR signal amplitude (middle three lines) for S1 samples containing a 20 µM solution of MmP in 2vol% DMSO and 98% ultrapure water (bottom). In the upper graph, the signal decrease of the middle peak at low doses is magnified.

The dose dependence of the determined A_n values for all S1 samples (3 per dose value) is depicted in Figure 6 (a). In the dose range from 0 to 16 Gy the dose dependent decrease of A_n can be described by a linear model ($A_n(D) = 1 - g \cdot D$ with a coefficient of determination of $R^2 = 0.997$) yielding a slope g of 0.02 per Gy. This translates into a nitroxide annihilation yield $G(-NO\cdot) = g/\rho \cdot c^0_{NO\cdot}$ of 0.4 µmol per Joule. At 16 Gy the remaining nitroxide concentration is about 13.6 µM. Beyond 16 Gy, the dose

dependence levels off, i.e. the slope g decreases as the dose increases. Consequently, $G(-NO\cdot)$ is apparently decreasing for nitroxide concentrations below 13.6 µM.

An exponential fit ($A_n(D) = exp\,(-kD)$ with $k = 0.028\ \mathrm{Gy}^{-1}$ and $R^2 = 0.988$) to the measured data points corresponding to the direct effect model derived in section 2.5 (equation (6)) yields the blue curve depicted in Figure 6 (a). According to equation (5), the fitted decay rate k translates into a nitroxide annihilation yield $G_{DE}(-NO\cdot)$ of 0.118 mol per Joule when the molecular mass of MmP (0.237 kg/mol) is used. $G_{DE}(-NO\cdot)$ obviously exceeds the yield $G(-NO\cdot)$ estimated from the initial constant slope between 0 Gy and 16 Gy by several orders of magnitude. This discrepancy indicates that the signal loss is not based on a direct effect.

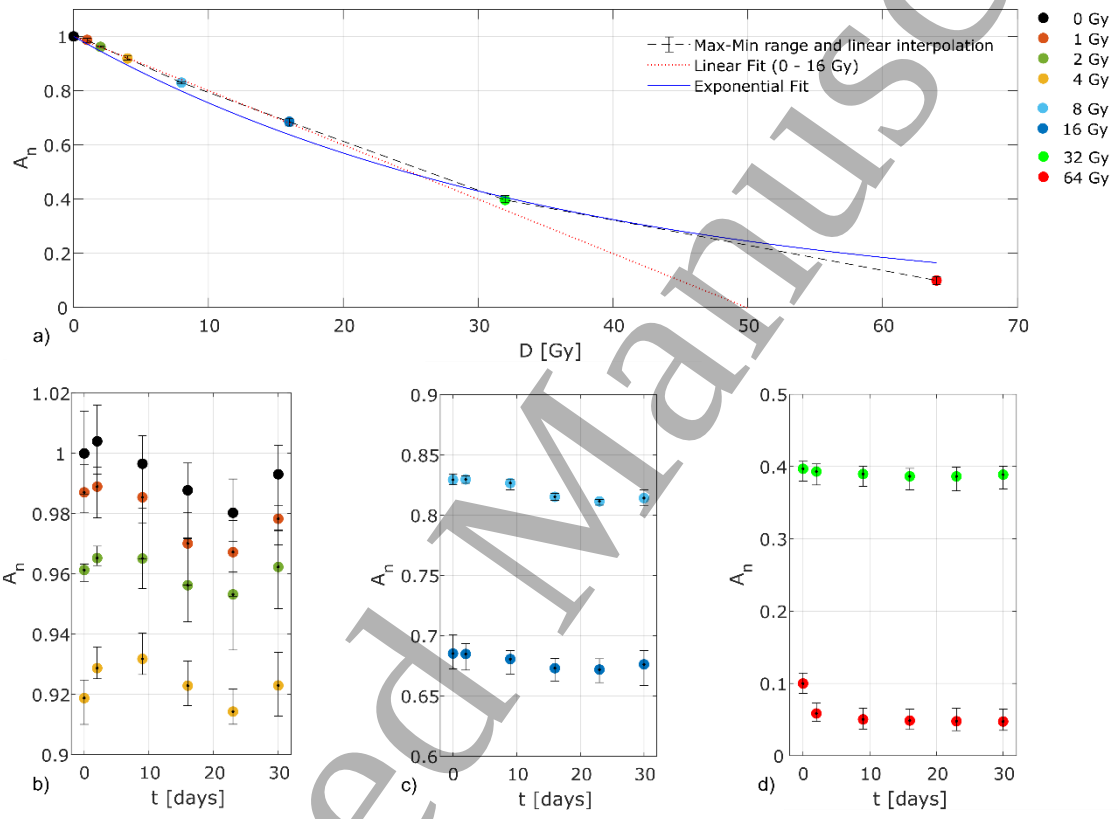

Figure 6. Dose dependence of normalized EPR signal amplitude A_n for S1 samples averaged over three samples per dose value (colored dot markers) measured on day 0 (day of irradiation). Linear and exponential fits (as described in the text) are plotted as red dotted line and blue solid line, respectively. A linear interpolation between data points is shown as black dashed line (a). Temporal stability of A_n for each dose value within five weeks following irradiation (b-c). For ~~both~~ all graphs, the uncertainty bars reflect the minimum and maximum values of three samples.

Figure 6 (b-d) shows the normalized EPR signal amplitudes obtained from repetitive measurements of three samples per dose value within five weeks following irradiation. The uncertainty bars indicate the maximum and minimum A_n value among three measured samples while the colored dots represent the mean A_n value per dose value. Table 1 shows the mean A_n values, standard deviations (*std*) and largest

deviations from the respective mean value (δ_{max}) determined over all six measurement days for each dose level. Within the investigated time period, a high stability of A_n values was observed for samples irradiated up to 32 Gy. For the 64 Gy samples, an initial signal decrease between day 0 and day 2 was noticeable. Excluding the 64 Gy samples, the relative standard deviation of A_n within 5 weeks (six measurements) following irradiation averaged over the remaining 21 samples (0 - 32 Gy) was 0.9% presenting a high level of signal stability and measuring reproducibility. Slight variations in the A_n values over time are visible in Figure 6 (b-d) and are presumably attributable to geometrical variations of the measuring setup. i.e. the exact positions of the Mn^{2+} reference and the guidance tube inside the resonator. Both parts were re-inserted into the resonator on each day of measurement.

		0 Gy	1 Gy	2 Gy	4 Gy	8 Gy	16 Gy	32 Gy	64 Gy
Over 3 samples									
mean(A_n)		0.994	0.980	0.960	0.923	0.821	0.679	0.390	0.059
std(A_n)		0.014	0.013	0.011	0.009	0.008	0.011	0.014	0.022
δ_{max}		-0.025	0.026	-0.025	-0.016	-0.014	0.019	0.023	0.055
Per Sample									
mean(A_n)									
	#1	0.983	0.971	0.950	0.927	0.822	0.672	0.409	0.064
	#2	1.009	0.976	0.961	0.915	0.823	0.691	0.380	0.043
	#3	0.988	0.992	0.971	0.927	0.818	0.672	0.382	0.069
std(A_n)									
	#1	0.008	0.009	0.009	0.006	0.007	0.003	0.003	0.022
	#2	0.005	0.009	0.005	0.006	0.009	0.006	0.006	0.020
	#3	0.011	0.009	0.004	0.007	0.008	0.009	0.003	0.014
δ_{max}									
	#1	-0.014	-0.014	-0.015	0.010	0.011	0.004	0.005	0.050
	#2	-0.009	0.014	-0.009	0.008	-0.013	-0.009	0.010	0.043
	#3	0.017	0.014	-0.006	-0.011	0.011	0.016	0.005	0.031

Table 1. A_n statistics table for measurement series S1. Mean values, standard deviations (*std*) and the largest deviations from the respective mean value (δ_{max}) are determined over all six measurement days.

For certain values of the parameter set, the indirect effect model derived in section 2.6 was applicable to describe the observed dose dependence $A_n(D)$ within the uncertainty bars (minimum and maximum values) of the measured data points (cf. Figure 7). Reaction channel 1 (cf. Figure 4) is responsible for the observed EPR signal loss due to nitroxide annihilation. The competing reaction channels 2 and 3 result in a decrease of the nitroxide annihilation per absorbed dose for decreasing nitroxide concentrations, i.e. at high cumulative doses. The initial slope of the dose dependence $A_n(D)$ is mainly influenced by model parameter $G(R\cdot)$, whereas the curvature is determined by the rate constants k_1, k_2 and k_3 and their

ratios. In the current work parameter values for two contrary scenarios are exemplarily presented: A) the nitroxides interact quickly (high rate constant k_1) with irradiation induced radicals $R_A\cdot$ being able to compete with reaction channel 2 (reaction between $R_A\cdot$ and the bulk solution). In this case the reaction between different $R_A\cdot$ radicals (channel 3) is very unlikely since the induced concentration per burst $[R_A\cdot]_b$ is too low to compete with reaction rates in channels 1 and 2; B) irradiation induced radical reactions with the bulk solution (channel 2) are completed before nitroxides react with the radical species $R_B\cdot$ arising therefrom. Rate constant k_1 is smaller than in scenario A, channel 2 is per assumption excluded and channel 3 is responsible for the flattening off of $[NO\cdot](D)$ at higher doses.

For scenario A, a reaction constant $k_1 = 5\cdot 10^8$ L mol^{-1}s^{-1} was chosen which can be reasonably assumed for the reaction between nitroxide radicals and carbon-centered radicals in water (Chateauneuf *et al.* 1988, Nigam *et al.* 1976). The radical concentration induced per photon burst $[R_A\cdot]_b$ was determined to be $4.7\cdot 10^{-4}$ µM resulting in a radical yield $G(R_A\cdot)$ of 0.59 µmol per Joule via equation (8). Given the relatively fast reactions via channel 1 and the low concentrations of $[R_A\cdot]_b$, reaction channel 3 had no influence on $[NO\cdot](D)$ even when high reaction rate constants in the order of $k_3 \approx 1\cdot 10^{10}$ L mol^{-1}s^{-1} (diffusion controlled limit) were assumed. The latter finding holds as long as $k_1 > 2\cdot 10^7$ L mol^{-1}s^{-1}. If this condition is met, the curvature of the resulting $[NO\cdot](D)$ depends on the ratio k_1/k_2. From the fit to the experimental data k_1/k_2 was determined to be $125\cdot 10^3$ L mol^{-1}. Accordingly, the rate constant k_2 was $4\cdot 10^3$ s^{-1}.

An example parameter set for scenario B was: $[R_B\cdot]_b = 3.6\cdot 10^{-4}$ µM resulting in a radical yield $G(R_B\cdot)$ of 0.45 µmol per Joule, $k_1 = 3\cdot 10^6$ L mol^{-1}s^{-1} and $k_3 = 7\cdot 10^9$ L mol^{-1}s^{-1}.

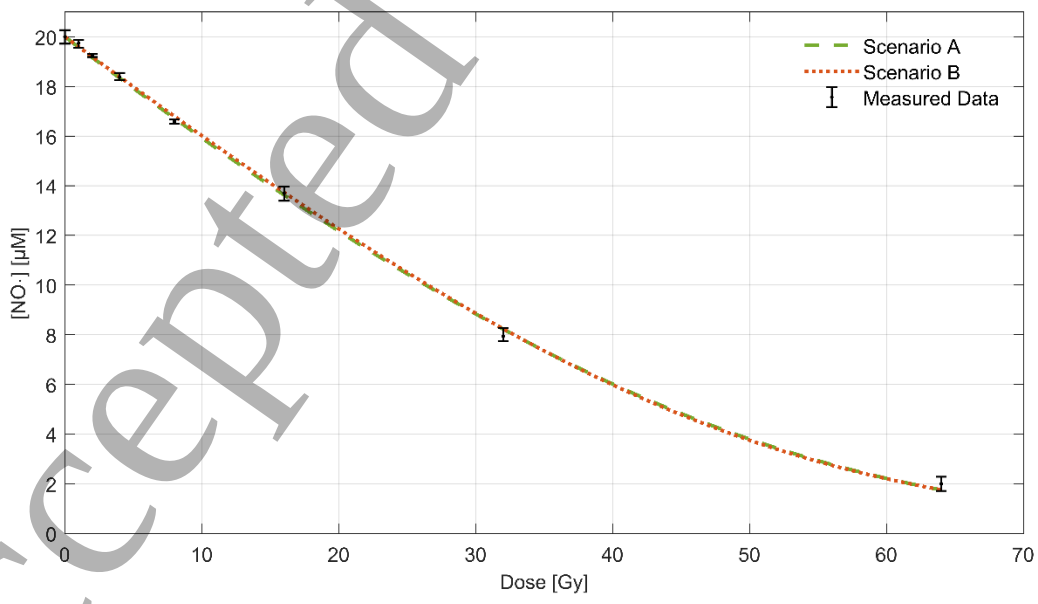

Figure 7. Simulated $[NO\cdot](D)$ curves resulting from the indirect effect model in case of a high (scenario A) or low (scenario B) rate constant k_1; For each scenario, model parameters $G(R\cdot)$, k_1, k_2 and k_3 were optimized such that $[NO\cdot](D)$ reflects the measured dose dependence.

Figure 7 shows the corresponding simulated $[NO\cdot](D)$ curves for both scenarios together with the measured data. For both scenarios, values of the model parameters can be optimized to result in virtually equal $[NO\cdot](D)$ curves that reflect the measured dose dependence.

3.2 Dependence on the initial nitroxide concentration $c^0_{NO\cdot}$

The results from measurement series S2 are depicted in Figure 8. As expected, the initial (0 Gy) A_n value increases linearly with the initial nitroxide concentration of the sample (Figure 8 (a), black circles). The EPR signal loss observed for different dose levels, however, does not proportionally increase with the initial nitroxide concentration but saturates at higher nitroxide concentrations $c^0_{NO\cdot}$ as shown in Figure 8 (a) and table 2. This observation is in contradiction to the predictions of the direct effect model (equation (7), section 2.5) and thus favors the indirect effect. A closer examination of the scattering of ΔA_n for five samples at each concentration level $c^0_{NO\cdot}$ was performed for the 16 Gy case and is shown in Figure 8 (b). Overall, an increase in the initial concentration leads to an increase in uncertainty of the determined ΔA_n value as depicted by the grey circles reflecting the relative standard deviation. At a concentration level of 20 µM a drop of relative uncertainty was observed.

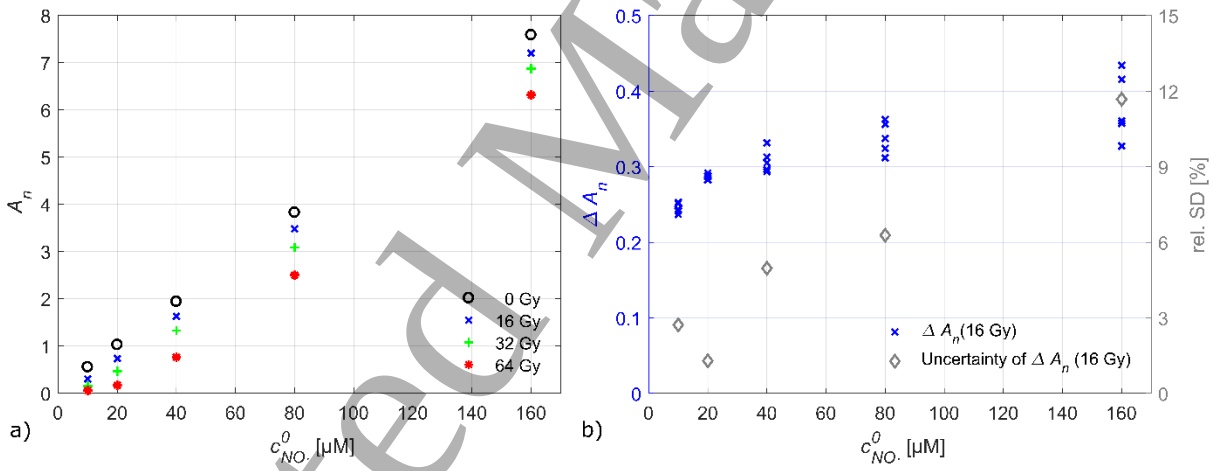

Figure 8. Results from measurement series S2: Dependences of the EPR signal amplitude A_n and of the irradiation induced signal loss on initial nitroxide concentration (a). Absolute EPR signal loss ΔA_n at 16 Gy and its uncertainty for different initial spin label concentrations estimated from the relative standard deviation of five sample measurements at each concentration level (b).

	$c^0_{NO\cdot}$ [µM]				
	10	20	40	80	160
ΔA_n(16 Gy)	0.25	0.29	0.31	0.35	0.39
ΔA_n(32 Gy)	0.41	0.56	0.61	0.74	0.72
ΔA_n(64 Gy)	0.50	0.86	1.18	1.33	1.27

Table 2. Signal loss ΔA_n observed in measurement series S2 for different initial nitroxide concentrations $c^0_{NO\cdot}$.

3.3 Dependence on DMSO concentration

Figure 9 shows the results obtained from the DMSO concentration measurement series S3. For zero DMSO concentration the irradiation induced EPR signal loss effect almost vanishes, i.e. ΔA_n < 0.04 at 16 Gy, while the signal loss rapidly increases for small amounts of DMSO. For example, ΔA_n is about 0.2 at 16 Gy for 0.2vol% DMSO concentration, i.e. about half that of 10vol% DMSO. This finding is the ultimate reason to reject the direct effect, since the corresponding model predicts a signal loss independently of the DMSO concentration. In contrast, the indirect effect model is applicable to explain the observed dependency: The increase of irradiation induced EPR signal loss with increasing DMSO concentration is due to an associated increase in the radical yield $G(R\cdot)$.

The increase of ΔA_n levels off for DMSO concentrations in the range of 2 - 10 vol%.

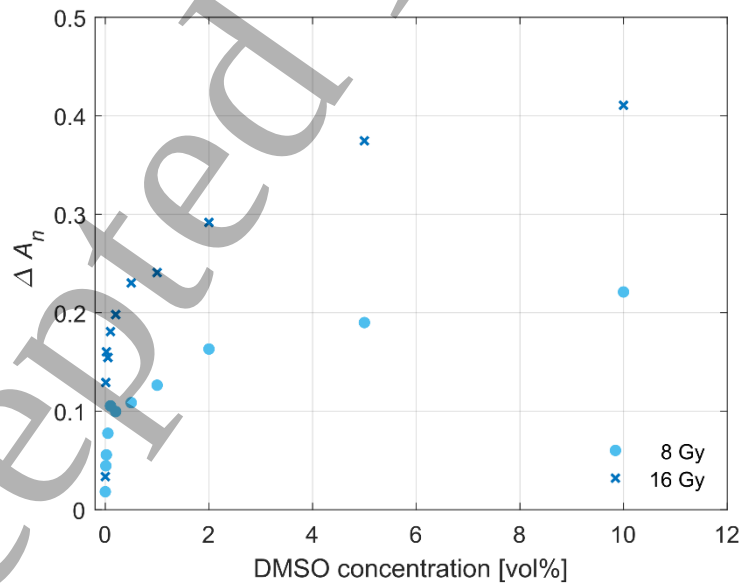

Figure 9. Results from measurement series S3: Dependence of the irradiation induced EPR signal loss ΔA_n on DMSO concentration for two dose levels (8 Gy and 16 Gy).

4. Discussion

The demonstrated fluid EPR dosimetry mixture fulfills basic requirements for dosimetry: monotonous dose response as well as high signal stability and reproducibility. Furthermore, the proposed aqueous solutions containing nitroxides in low concentration (20 µM) and small amounts of DMSO (2vol%) are virtually water equivalent and therefore provide promising potential for future dosimetry applications.

Water equivalence

In the present work, a DMSO concentration of 2vol% was mainly used. The resulting physical density of the water/DMSO mixture is close to water (< 1.002 kg/L). Figure 10 shows the energy dependence of the radiation transport properties ($\left(\frac{\mu_{en}}{\rho}\right)$ and $\left(\frac{S_{col}}{\rho}\right)$) relative to pure water for common EPR and thermoluminescence dosimeter materials in comparison to a 98vol%/2vol% water/DMSO mixture. The resulting radiation transport properties of the water/DMSO mixture are very close to unity throughout the energy range typically found in radiotherapy (shown as shaded area in Figure 10). Below a photon energy of 100 keV, i.e. for diagnostic X-ray energies, the ratio of the mass energy absorption coefficient relative to water increases but is below 1.1.

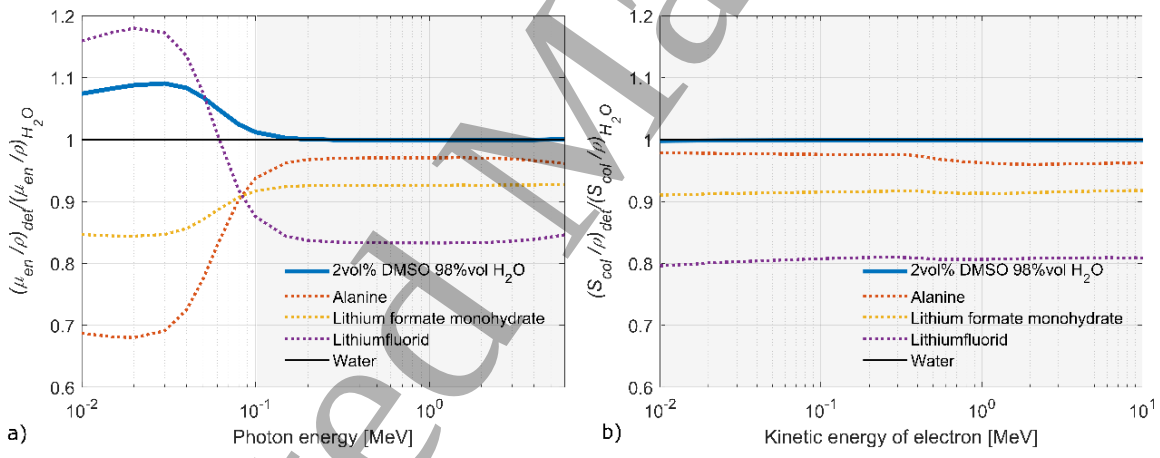

Figure 10. Energy dependence of radiation transport properties ($\left(\frac{\mu_{en}}{\rho}\right)$ and $\left(\frac{S_{col}}{\rho}\right)$) for different dosimeter materials relative to water. For a compound's $\frac{\mu_{en}}{\rho}$, listed mass energy absorption coefficients of the atomic constituents (Hubbell and Seltzer 2004) were weighted according to their fractions by weight and summed. Stopping powers were calculated with the ESTAR program (Berger *et al.* 2017).

Dose response and radiation yield

The irradiation induced change in radical concentration per absorbed dose, i.e. the radiation yield, is a key characteristic for a potential EPR dosimeter affecting its sensitivity (Lund *et al.* 2002). The typical X-ray radical yield (also known as G-value) of solid amino acids (such as ALA) commonly used for EPR dosimetry

is about 3 radicals per 100 eV of absorbed energy (Regulla and Deffner 1982) corresponding to approximately 0.3 µmol of generated radicals per Joule. The dose response observed in the present work is linear up to 16 Gy with a constant nitroxide annihilation yield $G(-NO\cdot)$ of 0.4 µmol per Joule when 20 µM initial nitroxide spin concentration and 2vol% DMSO is used. Note, however, that the radical formation in ALA dosimetry is rather based on direct effects in ALA molecules being predominantly present in solid pellets, whereas the radical annihilation yield of the current work was shown to be based on an indirect effect involving the nitroxide molecules in low concentration and radicals originating from the solvent molecules. Against this background, the observed magnitude of yield $G(-NO\cdot)$ is remarkable.

EPR signal stability

Nitroxides are well-known for their high thermodynamic stability in many solvents over a wide range of pH values at ambient conditions (Kokorin 2012). The results of measurement series S1 confirm a high degree of EPR signal stability of nitroxide solutions containing 2vol% DMSO, even after irradiation to doses of up to 32 Gy. Within the investigated time period of 30 days, i.e. six measurements within 5 weeks following irradiation, the largest relative deviation from the respective mean A_n value was below 2.6% for each sample (excluding the 64 Gy samples). In a previous study, nitroxides were used in aqueous solutions to detect free radical reactions after low linear energy transfer irradiation to doses of 16 Gy (Matsumoto *et al.* 2009). The authors found that the nitroxide concentration is decreased upon irradiation if hydrogen donor molecules like glutathione were present in the solution. However, temporal stability, even for the non-irradiated reaction mixture, was limited at room temperature. In the present study, an irradiation induced signal loss was mediated by DMSO as an additive to the aqueous solution maintaining high signal stabilities for doses up to 32 Gy. For the 64 Gy samples, an initial signal decrease was observed which was not further elucidated.

EPR signal reproducibility and dose uncertainty

Besides dose response and temporal signal stability, measurement reproducibility and the resulting dose uncertainty are important characteristics for a dosimetry method applied in radiotherapy. By optimizing sample positioning reproducibility, equalizing measuring conditions and applying spectral fitting for evaluation (cf. section 2.3-4), a high reproducibility (mean signal fluctuations of about 0.9%) for A_n could be achieved (64 Gy samples excluded). This value is to be seen as a benchmark for future improvements. The reproducibility was presumably affected by setup variations (e.g. small positional changes of the capillaries between measurements and small positional changes of the manganese reference inside the resonator between measuring days) on the one hand and slight inter-sample signal variations due to variations in the capillary inner diameter (cf. section 2.4) on the other, rather than signal fading effects. The estimated signal reproducibility is similar to ALA signal amplitude variations at 20 Gy (about 0.7%)

obtained with the same spectrometer previously (Höfel *et al.* 2021). However, higher reproducibility requirements and a more complicated analysis apply for the dosimetry approach introduced here due to the following reasons: The absolute signal decrease ΔA_n increases with the absorbed dose. Consequently, if a signal difference ΔA_n is used as measure for dosimetry, the dose uncertainty is depending on the uncertainty of two instead of one amplitude values A_n. Moreover, absolute EPR signal uncertainties increase with increasing A_n while relative uncertainties are rather constant throughout the intensity range investigate in this work. Since both the initial and the post-irradiation A_n value as well as their absolute uncertainties depend on $c^0_{NO\cdot}$, $c^0_{NO\cdot}$ has to be carefully and precisely adjusted depending on the desired dose range and dose uncertainty level. This issue should be addressed in more detail by future studies. In the present study, the uncertainty of ΔA_n at 16 Gy was examined for different $c^0_{NO\cdot}$ ranging from 10 µM to 160 µM by the measurement of five samples. As an overall trend, it could be shown that the uncertainty given as relative standard deviation decreases for lower $c^0_{NO\cdot}$. The observed drop for $c^0_{NO\cdot} = 20$ µM is presumably based on a better spectral fitting performance (cf. section 2.4), since the base spectrum R^B was acquired with the same nitroxide concentration of 20 µM and the spectral linewidth is slightly depending on the nitroxide concentration due to Heisenberg exchange and dipolar interactions (Bales *et al.* 2009). For a nitroxide concentration in the range of 10 - 20 µM and a DMSO concentration of 2vol%, the expected relative dose uncertainty at the 16 Gy level would be in the order of 3% for the experimental procedure applied in this work. At lower doses or at higher initial concentrations, the relative dose uncertainty is expected to increase.

Concentration dependencies indicating an indirect effect

Measurement series S2 and S3 were conducted to investigate the dependence of the EPR signal loss on $c^0_{NO\cdot}$ and DMSO concentration, respectively. The obtained results provide several fundamental insights regarding possibilities to enhance the signal loss effect and the nature of the underlying mechanism. In summary, only a small dependence on $c^0_{NO\cdot}$ but a strong dependence on the DMSO concentration, especially between 0-5 vol%, was observed. These results support the indirect nature of the signal loss mechanism: i) The absolute signal loss did not proportionally increase with increasing $c^0_{NO\cdot}$ as predicted by the direct effect model (equation (7)), ii) The signal loss effect rapidly decreases when the DMSO concentration approaches zero. Further experimental evidence is provided by the dose dependence of A_n: iii) The course of the measured data could be described by the indirect effect model rather than by an exponential fit as expected from the direct effect model, iv) the yield $G_{DE}(-NO\cdot)$ resulting from an exponential fit using the direct model exceeded the experimentally determined annihilation yield $G(-NO\cdot)$ of 0.4 µmol per Joule by several orders of magnitude. It is generally well accepted that in dilute solutions (concentrations lower than 1 mM) the direct ionization of solute molecules is negligible since most of the radiation energy is absorbed by the solvent (Ma *et al.* 2019).

Modelling the indirect effect

The established indirect effect model could be successfully applied to reflect the measured dose dependence of A_n. Two contrary scenarios (A and B) were examined that can result in virtually equal EPR signal loss predictions. As a consequence, based on the current study an unique set of values for the parameters of the proposed model cannot be provided. Hence, the modelling of the indirect effect needs further detailed investigations in future research.

The role of DMSO

This work provides strong evidence that DMSO acts like a mediator for the EPR signal loss observed in the present study. DMSO is often applied as a scavenger for the OH· radical providing diffusion-controlled reaction rate constants (Meissner *et al.* 1967, Reuvers *et al.* 1973). It was shown by Meissner *et al.* that a concentration of about 5 vol% DMSO is sufficient to scavenge almost all irradiation induced OH· radicals in aqueous solution. Likewise in the current work, the increase in ΔA_n levels off around 5 vol% DMSO which supports the explanation following the OH· scavenging pathway that may result in different reactive radical species (Ashwood-Smith 1975, Gilbert *et al.* 1975, Veltwisch *et al.* 1980, Koulkes-Pujo *et al.* 1982, Eberhardt and Colina 1988, Babbs and Griffin 1989, Steiner and Babbs 1990, Flyunt *et al.* 2001). Thus, different radical products can be formed via the radiolysis of water/DMSO mixtures depending on oxygen level and pH. At the current stage, we can only speculate about the exact mechanism underlying the indirect effect.

Yet there is still the possibility that ionizations directly occurring in DMSO lead to DMSO derived radicals that may contribute dominantly to the observed signal loss effect (Stevanovic *et al.* 2012). However, assuming a decomposition yield of DMSO of 0.67 µmol per Joule (Gutierrez and Barrera 1978) and a DMSO concentration of 2vol% (0.28 M) the number of decomposed DMSO molecules per Gray of absorbed dose is only 0.015 µM following equation (7), i.e. much smaller than the observed nitroxide annihilation yield $G(-NO\cdot)$. Moreover, it has been shown previously that direct effects in DMSO play a minor role for DMSO concentrations below 10vol% (Koulkes-Pujo *et al.* 1982).

In summary, the experimental results provide evidence that an indirect effect mediated by DMSO is the underlying mechanism for the observed signal loss of nitroxides in aqueous solution.

Limitations

Experiments in this study were conducted with a clinical radiotherapy beam (6 MV FFF photon beam in pulsed mode with a repetition frequency of 167 Hz, a pulse (burst) duration of approximately 4.2 µs (FWHM) and a dose per burst of about 0.8 mGy). The influences of beam parameters (e.g. dose rate) were not considered in the current work but will be addressed in future work.

In the present work, the same encapsulation (glass capillaries) was used for EPR readout and irradiation. In future work, the encapsulation during irradiation could be replaced by a more water equivalent material in terms of physical density and atomic composition.

The applied indirect effect model is a heuristic and simplified approach of modeling irradiation induced radical reaction kinetics between the solvent (water/DMSO mixture) and the EPR active solute molecules (nitroxides). While this model was applicable to describe the dependencies revealed by the measurement series S1, it was assumed that a single radical species $R\cdot$ is formed by the radiolysis of the water/DMSO mixture that may react via a very limited number of (three) reaction channels.

5. Conclusion

The results of the present work demonstrate the use of nitroxides in aqueous solution containing small amounts of DMSO as potential future EPR dosimeter material by following a novel signal loss approach. The tested nitroxide solution (20 µM MmP in 2vol% DMSO and 98% ultrapure water) fulfills basic requirements for passive dosimeters such as high water equivalence, a monotonous dose response, low post-irradiation signal fading rate and a high measurement reproducibility. At the current experimental stage, a dose uncertainty of about 3% could be achieved at a dose level of 16 Gy. More research is required regarding signal loss enhancement in order to decrease uncertainties at lower doses. A volume fraction of 2vol% DMSO is a reasonable choice for maximizing the dose response while maintaining a high level of water equivalence in terms of the radiation transport properties $\left(\frac{\mu_{en}}{\rho}\right)$ and $\left(\frac{S_{col}}{\rho}\right)$ as well as density. The concentration dependencies of the dose response together with the established model predictions show that an indirect effect of irradiation causes the observed EPR signal loss. Thus, the results of this study suggest that the signal loss is mediated by diffusing radicals originating from the radiolysis of the water/DMSO mixture.

The current work constitutes a starting point for future research on liquid, water-equivalent EPR dosimeters. Besides water equivalence, other advantages over traditional solid EPR dosimeters could be: i) easy deformability, ii) small volume (≈25 µL), iii) high batch and sample homogeneity, iv) equalization of inhomogenous dose deposition via diffusion. There are many interesting applications and test scenarios for liquid, water-equivalent EPR dosimeters such as dosimetry in small radiation fields or dosimetry near the surface, i.e. in the dose build-up region.

Acknowledgements

The authors would like to thank the following former students for their contributions to the method development: Michael Stehle, Maximilian Mattes, Jakob Haber and Kim Gmeiner. Special thanks to the working group members Lara Williams, Eva Schaefer and Dr. Mykhailo Azarkh for their support and helpful discussions. We would further like to thank Prof. Dr. Adelheid Godt from the University of Bielefeld for in-depth discussions on possible reaction mechanisms.

Conflicts of Interest

All authors disclose any potential conflict of interest.

References

Almond P R, Biggs P J, Coursey B M, Hanson W F, Huq M S, Nath R and Rogers D W O 1999 AAPM's TG-51 protocol for clinical reference dosimetry of high-energy photon and electron beams *Medical Physics* 26 1847–70

Alpen E L 1998 Chapter 7 - Theories and Models for Cell Survival Radiation Biophysics (Second Edition) ed E L Alpen (San Diego: Academic Press) pp 132–68 Online: https://www.sciencedirect.com/science/article/pii/B9780120530854500090

Anton M 2005 Development of a secondary standard for the absorbed dose to water based on the alanine EPR dosimetry system *Applied Radiation and Isotopes* 62 779–95

Anton M 2008 Postirradiation effects in alanine dosimeter probes of two different suppliers *Phys. Med. Biol.* 53 1241

Antonovic L, Gustafsson H, Carlsson G A and Tedgren Å C 2009 Evaluation of a lithium formate EPR dosimetry system for dose measurements around I192r brachytherapy sources *Medical Physics* 36 2236–47

Apipunyasopon L, Srisatit S and Phaisangittisakul N 2013 An investigation of the depth dose in the build-up region, and surface dose for a 6-MV therapeutic photon beam: Monte Carlo simulation and measurements *Journal of Radiation Research* 54 374–82

Ashwood-Smith M J 1975 Current Concepts Concerning Radioprotective and Cryoprotective Properties of Dimethyl Sulfoxide in Cellular Systems* *Annals of the New York Academy of Sciences* 243 246–56

Babbs C F and Griffin D W 1989 Scatchard analysis of methane sulfinic acid production from dimethyl sulfoxide: A method to quantify hydroxyl radical formation in physiologic *systems Free Radical Biology and Medicine* 6 493–503

Bales B L, Meyer M, Smith S and Peric M 2009 EPR Line Shifts and Line Shape Changes due to Spin Exchange of Nitroxide Free Radicals in Liquids: 6. Separating Line Broadening due to Spin Exchange and Dipolar Interactions *J. Phys. Chem. A* 113 4930–40

Berger M J, Coursey J S, Zucker M A, Chang J 2017 NIST standard reference database 124. Stopping-Power & Range Tables for Electrons, Protons, and Helium Ions. Last update to data content: July 2017. doi: https://dx.doi.org/10.18434

Bordignon E 2017 EPR Spectroscopy of Nitroxide Spin Probes eMagRes (*American Cancer Society*) pp 235–54 Online: https://onlinelibrary.wiley.com/doi/abs/10.1002/9780470034590.emrstm1513

Chateauneuf J, Lusztyk J and Ingold K U 1988 Absolute rate constants for the reactions of some carbon-centered radicals with 2,2,6,6-tetramethyl-1-piperidinoxyl *J. Org. Chem.* 53 1629–32

Chofor N, Harder D and Poppe B 2012 Non-reference condition correction factor kNR of typical radiation detectors applied for the dosimetry of high-energy photon fields in radiotherapy *Zeitschrift für Medizinische Physik* 22 181–96

Cronholm R O, Andersen C E, Behrens C F and Helt-Hansen J 2012 Volume dose ratios relevant for alanine dosimetry in small, 6 MV photon beams. *Radiation Measurements* 47 1014–7

Distefano G, Lee J, Jafari S, Gouldstone C, Baker C, Mayles H and Clark C H 2017 A national dosimetry audit for stereotactic ablative radiotherapy in lung. *Radiotherapy and Oncology* 122 406–10

Eberhardt M K and Colina R 1988 The reaction of OH radicals with dimethyl sulfoxide. A comparative study of Fenton's reagent and the radiolysis of aqueous dimethyl sulfoxide solutions *J. Org. Chem.* 53 1071–4

Desrosiers M F, Puhl J M, and Cooper S L 2008 An Absorbed-Dose/Dose-Rate Dependence for the Alanine-EPR Dosimetry System and Its Implications in High-Dose Ionizing Radiation Metrology. *Journal of Research of the National Institute of Standards and Technology* Volume 113

Fenwick J D, Kumar S, Scott A J D and Nahum A E 2013 Using cavity theory to describe the dependence on detector density of dosimeter response in non-equilibrium small fields *Phys. Med. Biol.* 58 2901

Flyunt R, Makogon O, Schuchmann M N, Asmus K-D and Sonntag C von 2001 OH-Radical-induced oxidation of methanesulfinic acid. The reactions of the methanesulfonyl radical in the absence and presence of dioxygen *J. Chem. Soc., Perkin Trans.* 2 787–92

Gargett M A, Briggs A R and Booth J T 2020 Water equivalence of a solid phantom material for radiation dosimetry applications *Physics and Imaging in Radiation Oncology* 14 43–7

Gilbert B, Norman R O and Sealy R 1975 Electron spin resonance studies. Part XLIII. Reaction of dimethyl sulphoxide with the hydroxyl radical *Journal of the Chemical Society, Perkin Transactions* 2 0 303–8

Gutierrez M C and Barrera R 1978 Gamma-radiolysis of dimethyl sulfoxide II Radiolysis yields and possible mechanisms Report 424 of the *Junta de Energia Nuclear (JEN)*, Madrid (Spain)

Höfel S, Stehle M, Zwicker F, Fix M K and Drescher M 2021 A practical EPR dosimetry system for routine use in radiotherapy: uncertainty analysis of lithium formate dosimeters at the therapeutic dose level *Phys. Med. Biol.* 66 045005

Hubbell J H, Seltzer S M 2004 NIST standard reference database 126. X-ray mass attenuation Coefficients. Last update to data content: July 2004. doi: https://dx.doi.org/10.18434

IAEA 2001 Technical Report Series No. 398. Absorbed Dose Determination in External beam radiotherapy: An International Code of Practice for Dosimetry based on Standards of Absorbed Dose to Water. (Vienna: International Atomic Energy Agency.) Online: https://www.iaea.org/publications/5954/absorbed-dose-determination-in-external-beam-radiotherapy

ICRU 1989. Report 44. Tissue substitutes in radiation dosimetry and measurement. *International Commission on Radiation Units and Measurements*, Bethesda, MD, USA.

Kokorin A I 2012 Nitroxides - Theory, Experiment and Applications Online: https://www.intechopen.com/books/2507

Koulkes-Pujo A M, Moreau M and Sutton J 1982 Radiolytic reduction of ceric salts in water-dimethyl sulfoxide mixtures and pure dimethyl sulfoxide. Contribution to the study of the direct effect *J. Phys. Chem.* 86 1421–6

Lund A, Olsson S, Bonora M, Lund E and Gustafsson H 2002 New materials for ESR dosimetry *Spectrochim Acta A Mol Biomol Spectrosc* 58 1301–11

Ma J, Denisov S A, Adhikary A and Mostafavi M 2019 Ultrafast Processes Occurring in Radiolysis of Highly Concentrated Solutions of Nucleosides/Tides *Int J Mol Sci* 20 Online: https://www.ncbi.nlm.nih.gov/pmc/articles/PMC6801490/

Ma C-M and Li J 2011 Dose specification for radiation therapy: dose to water or dose to medium? *Phys. Med. Biol.* 56 3073

Matsumoto K-I, Okajo A, Nagata K, Degraff W G, Nyui M, Ueno M, Nakanishi I, Ozawa T, Mitchell J B, Krishna M C, Yamamoto H, Endo K and Anzai K 2009 Detection of free radical reactions in an aqueous sample induced by low linear-energy-transfer irradiation *Biol. Pharm. Bull.* 32 542–7

Meissner G, Henglein A and Beck G 1967 Pulsradiolytische Untersuchung von Dimethylthioäther und Dimethylsulfoxyd in wäßriger Lösung *Zeitschrift für Naturforschung* B 22 13–9

Nahum A E 1996 Perturbation effects in dosimetry: Part I. Kilovoltage x-rays and electrons *Phys. Med. Biol.* 41 1531

Nigam S, Asmus K-D and Willson R L 1976 Electron transfer and addition reactions of free nitroxyl radicals with radiation induced radicals *J. Chem. Soc., Faraday Trans.* 1 72 2324

Olsen K J, Hansen J W and Wille M 1990 Response of the alanine radiation dosemeter to high-energy photon and electron beams *Phys. Med. Biol.* 35 43–52

O'Shea E and McCavana P 2003 Review of surface dose detectors in radiotherapy *Journal of Radiotherapy in Practice* 3 69–76

Papanikolaou N, Battista J, Boyer A, Klein E and Sharpe M 2004 Tissue inhomogeneity corrections for megavoltage photon beams *AAPM Task Group* 85

Poppinga D, Delfs B, Meyners J, Harder D, Poppe B and Looe H K 2018 The output factor correction as function of the photon beam field size – direct measurement and calculation from the lateral dose response functions of gas-filled and solid detectors *Zeitschrift für Medizinische Physik* 28 224–35

Regulla D F and Deffner U 1982 Dosimetry by ESR spectroscopy of alanine *The International Journal of Applied Radiation and Isotopes* 33 1101–14

Reuvers A P, Greenstock C L, Borsa J and Chapman J D 1973 Studies on the Mechanism of Chemical Radioprotection by Dimethyl Sulphoxide International *Journal of Radiation Biology and Related Studies in Physics, Chemistry and Medicine* 24 533–6

Schaeken B, Cuypers R, Lelie S, Schroeyers W, Schreurs S, Janssens H and Verellen D 2011 Implementation of alanine/EPR as transfer dosimetry system in a radiotherapy audit programme in Belgium *Radiotherapy and Oncology* 99 94–6

Sharpe P H G, Rajendran K and Sephton J P 1996 Progress towards an alanine/ESR therapy level reference dosimetry service at NPL *Applied Radiation and Isotopes* 47 1171–5

Soule B P, Hyodo F, Matsumoto K, Simone N L, Cook J A, Krishna M C and Mitchell J B 2007 Therapeutic and Clinical Applications of Nitroxide Compounds *Antioxidants & Redox Signaling* 9 1731–44

Steiner M G and Babbs C F 1990 Quantitation of the hydroxyl radical by reaction with dimethyl sulfoxide *Archives of Biochemistry and Biophysics* 278 478–81

Stevanovic S, Miljevic B, Eaglesham G K, Bottle S E, Ristovski Z D and Fairfull‐Smith K E 2012 The Use of a Nitroxide Probe in DMSO to Capture Free Radicals in Particulate Pollution *European Journal of Organic Chemistry* 2012 5908‐12

Torricella F, Pierro A, Mileo E, Belle V and Bonucci A 2020 Nitroxide spin labels and EPR spectroscopy: a powerful association for protein dynamics studies *Biochimica et Biophysica Acta (BBA) - Proteins and Proteomics* Online: https://hal.science/hal-03441104

Veltwisch D, Janata E and Asmus K-D 1980 Primary processes in the reaction of OH··radicals with sulphoxides *Journal of the Chemical Society, Perkin Transactions* 2 0 146–53

Vestad T A, Malinen E, Olsen D R, Hole E O and Sagstuen E 2004 Electron paramagnetic resonance (EPR) dosimetry using lithium formate in radiotherapy: comparison with thermoluminescence (TL) dosimetry using lithium fluoride rods *Phys. Med. Biol.* 49 4701

Waldeland E, Helt-Hansen J and Malinen E 2011 Characterization of lithium formate EPR dosimeters for high dose applications – Comparison with alanine *Radiation Measurements* 46 213–8

Webb A 2014 Cavity- and waveguide-resonators in electron paramagnetic resonance, nuclear magnetic resonance, and magnetic resonance imaging *Progress in Nuclear Magnetic Resonance Spectroscopy* 83 1–20